Original research article

Mechanical property of YCF101 coating under different overlap modes by laser cladding

Yu Zhao[a,b], Liaoyuan Chen[a,b], Jiayu Sun[c], Tianbiao Yu[a,b,*]

[a] School of Mechanical Engineering and Automation, Northeastern University, Shenyang, 110819, China
[b] Liaoning Provincial Key Laboratory of High-end Equipment Intelligent Design and Manufacturing Technology, Northeastern University, Shenyang, 110819, China
[c] Deformation Processing Institute for Materials Research, Tohoku University, Sendai, 980-8577, Japan

ARTICLE INFO

ABSTRACT

The specimens with three different overlap modes were successfully manufactured. The mechanical properties of the clad layer were measured along the scanning direction and z-axis direction respectively. The results show that the increased uniformity of remelting temperature distribution made the cracks and pores decreased and the microstructure refined. The coatings had a ower friction coefficient, and shallow and narrow scratch along the scanning direction. YCF101 alloy is a plastic material and the compressive property of the clad layer was improved by the uniformity of grain. Improving the consistency of the clad track and the loading direction can improve the coating compressive performance.

1. Introduction

China has become one of the world's largest numbers of used machine tools, of which more than 2.2 million old traditional machine tools over 10 years of service, 80 % are overdue service. The remanufacturing of machine tool parts plays an important role in the industrialization and scale of the remanufacturing process of used machine tools. The choice of the laser repairing powder is a crucial link in laser repairing of waste parts. Fe-based alloys have many advantages that cannot be ignored, such as abundant reserves, low cost and good compatibility with machine tool components. However, at present, the physical properties of Fe-based alloy powders are seldom studied and there is no standard of physical parameters. To some extent, it also hinders the application of Fe-based alloy powder in industry. Therefore, it is urgent to study the properties of Fe-based coating using laser cladding technology [1–3].

Many scholars have studied the laser cladding process parameters and the application of Fe-based alloy [4–9]. In the research of laser cladding parameters, Weng et al. [10] investigated the interfacial behavior about laser repairing of V-grooves using Fe-based alloy powder under different parameters. The high laser power would cause cracking in the interfacial region. The microhardness in the cladding area is much higher than that of the substrate. Jiao et al. [11] illustrated the effects of laser scanning speed on the wear resistance and microstructure of T15 M (Fe-based) coating. They found that the scanning speed is not monotonic to wear resistance, and the coating was fabricated under the scanning speed of 200 mm/min has the best wear resistance. Lyu et al. [4] investigated the wear resistance of the coatings which injects B_4C on the center and the edge of the melting pool. The results showed that the wear resistance increased with the existence of B_4C particles. Guo et al. [5] studied the evolution of the nanostructured bainite in full

nanobainitic coatings. They fabricated fully nanobainitic coatings with low dilution and no cracks and pores, and revealed that the bainite grew with a diffusionless mechanism. Gao et al. [12] analyzed the effect of the beam in a positive and negative defocused zone on the Fe-based coating. They found that negative defocus can reduce the dilution rate and pores. In order to improve the wear and corrosion resistance, Fan et al. [6] developed two novel Fe-based alloy coatings. The results showed that the Fe-Cr(Ni) solid solution can improve the microhardness of the coating and the mild abrasive wear was the dominant wear mechanism of the Fe-based alloy coating, and the high Cr and Ni content can improve the coating corrosion resistance. In the above studies, few works have been conducted on the physical properties of Fe-based alloy, mainly on the improvement of the coating properties and the effect of process parameters on the properties of the alloy coatings, which also affects the application of Fe-based alloy in the industry.

In application, Roy et al. [13] investigated the influence of cladding materials (410 L stainless steel, SS420 stainless steel and Stellite 6) and heat treatment process on the rails. Fu et al. [14] used the rolling-sliding device to measure the microstructure and wear resistance of Fe-based alloy coating which has been fabricated on wheel/rail materials. Xu et al. [15] investigated the re-manufacturing process of failure thin-wall impeller blade with FeCrNiCu alloy powder using laser cladding. Lin [16] used the optimal laser processing parameters to repair a turbine blade tenon. The repaired tenon can bear a 30 K N tensile load.

In recent years, in order to enhance the properties of Fe-based alloys and expand their usability, many scholars studied the effects of Fe-based composite coatings on its properties [17–23]. In our lab, we also studied the influence of laser processing parameters and Fe-based composite coating on its properties [24–26]. Duo to the lack of physical parameters of Fe-based alloys, the research of Fe-based alloy powder is not systematic and there is no uniform standard. The different overlap methods have a direct impact on the remelting zone, temperature gradient distribution, metallurgical bonding quality of coating, etc. Therefore, based on previous studies, this paper will continue to study the properties of YCF101 alloy powder. In this study, three different overlap modes were used to investigate the wear resistance and compressive strength of the YCF101 alloy coatings. The coating performance is studied from the direction of lifting and parallel lifting respectively.

2. Experimental

2.1. Process parameters and cladding system

Cladding parts with different overlap modes on the 45 substrate using laser cladding technology were fabricated. The composition of 45 steel plate and YCF101 alloy is shown in Table 1.

The experimental equipment is an open-loop control system as shown in Fig. 1 [27].

The cladding process parameters of YCF101 powder alloy which got by experiments are shown in Table 2.

2.2. Process design

In order to homogenize the microstructure and improve the metallurgical bonding ability between the clad tracks, three different overlap modes were designed, as shown in Fig. 2. Fig. 2(a) is the three different overlap modes. Mode 1: the cladding methods of each layer are 'bow shaped'; mode 2: the 'bow shaped' scanning direction of the adjacent two layers perpendicular to each other; mode 3: the angle of scanning direction between the first layer and second layer is 90°, the angle of the third layer and the second layer is 45°, the angle of the fourth layer and third layer is 90°. According to three different modes, the cuboid was fabricated with a size of 35 mm × 25 mm × 15 mm as shown in Fig. 2(b). The compressive and wear resistance specimens were prepared along the long direction and high direction of the cuboid, respectively. The size of the compressive specimen is 6 mm × 6 mm × 18 mm, and the microhardness specimen is 10 mm × 10 mm × 5 mm, as shown in Fig. 2(c).

All specimens were sanding with different types of sandpaper, and the microhardness measurement specimens should be polished and then corroded with corrosive solution (HCl: H_2O: $FeCl_3$ = 20:10:1) 5–10S. The laser confocal microscope (LEXTOLS4100) was used to observe the microstructure and cross-section overlapping morphology. The universal testing machine was used to measure the specimens of different overlap modes, and the compression rate is 2 mm/min. The effect of the different overlaps on the wear resistance of the specimen was analyzed by wear tester MFT-4000, the test load is 10 N, the wear time is 100 min, the reciprocating distance is 5 mm, the speed is 200 mm/min, and the milling ball is φ 5 GCr15.

2.3. Trajectory optimization design

The off-line software RobotArt was used to generate Robot code, the specific optimization process is shown in Fig. 3. First, the robot (KUKA16-3), tool (laser cladding head) and parts should be imported in turn. The relative position of the tool and the robot, and the relative position of the robot and the parts should be determined, that is, the TCP point setting and the workpiece calibration. To

Table 1
Chemical composition (wt%) of 45 steel and YCF101 steel powder (provided by suppliers).

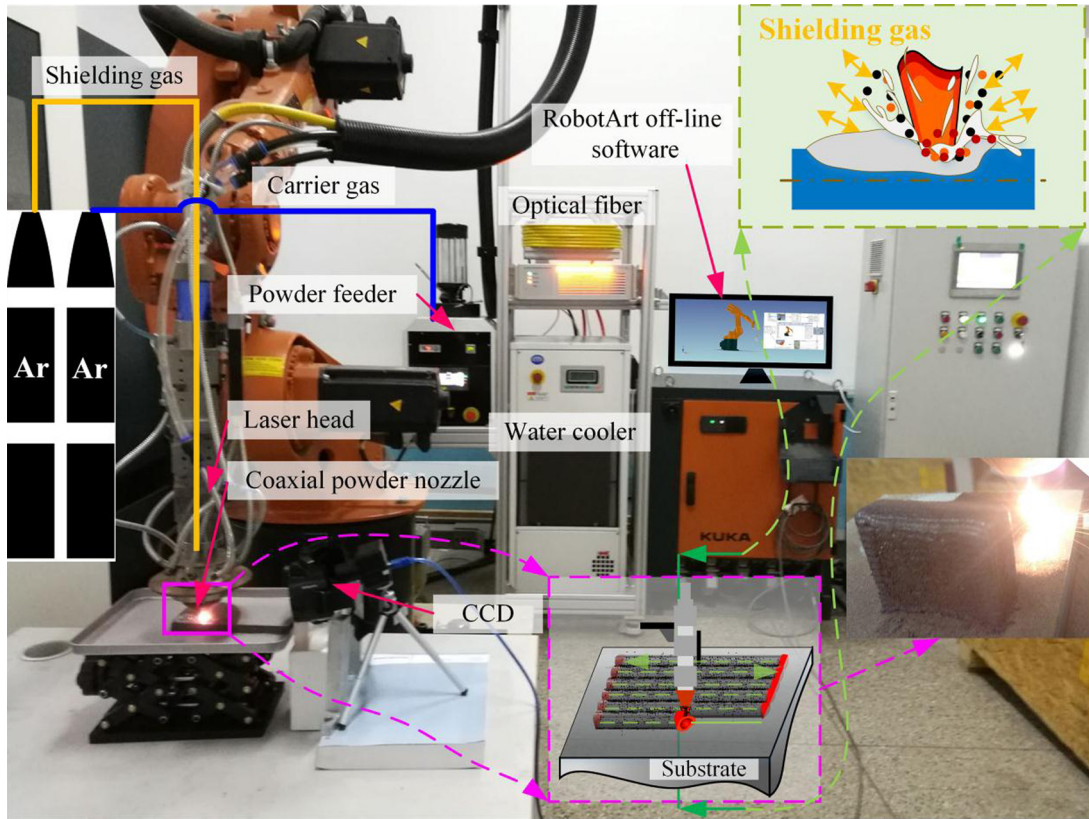|	C	B	P,S	Si	Cr	Ni	Mn	Mo	Nb	Cu	N	Fe
RCF101	0.05	0.22	–	0.9	15.5	6.5	0.4	1	0.31	–	0.2	Bal.
45 steel	0.42 − 0.5		≤0.045	0.17 − 0.37	≤0.25	≤0.25	0.5 − 0.8	–	–	≤0.25	–	Bal.

Fig. 1. Laser cladding system.

Table 2
Optimal operating parameters for multi-layer DLF of YCF101 alloy powder.

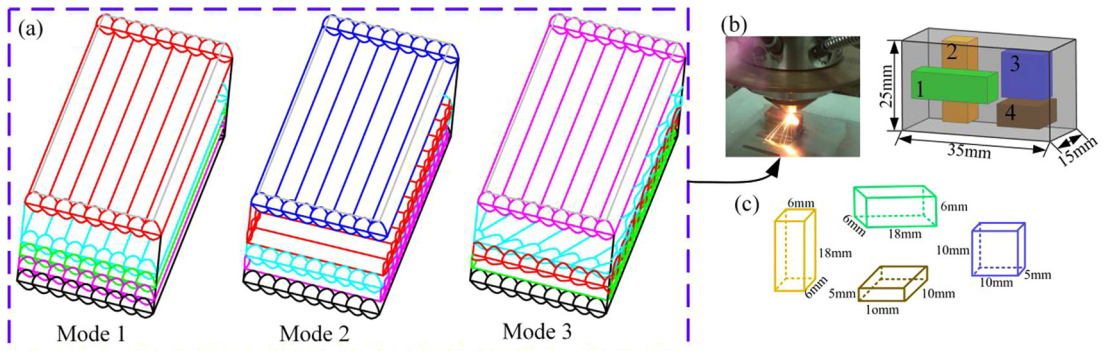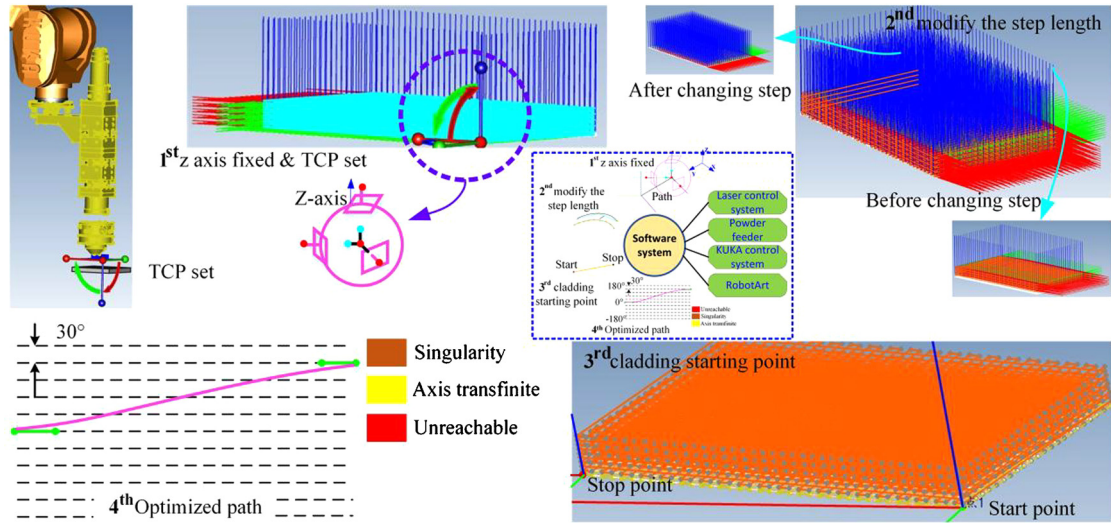| Process parameter	Value	Unit
Laser power	450	W
Scanning speed	0.55	mm/s
Powder feeding rate	9.10	g/min
Track spacing	0.9	mm
Z-axis increasing	0.35	mm
Sending powder gas	6	L/h
Shielding gas	12	L/h

Fig. 2. Experiment design.

Fig. 3. Trajectory optimization.

ensure the stability of the laser head movement which is driven by a robot, so the z-axis should be fixed. Second, if the curve appears in the trajectory, the step length should be set reasonably to ensure that the simulation trajectory can be closer to the design trajectory. The too-large step length would cause bad deviated between the simulation trajectory and the actual running trajectory. The too-small step length could guarantee the coincidence between the simulation trajectory and the design trajectory, but it increases the number of trajectory points. The lengthy post-processing procedures will increase the workload. In this paper, all the trajectories are straight line without taking into account the choice of step length. Third, the position of the starting point and stopping point is chosen in the principle of the starting points evenly distributed around the trajectories; Forth, in order to improve the stability and safety of the cladding process, the trajectory optimization is mainly to keep the rotation angle of the laser cladding head and the KUKA end-effector between ± 0.5. And then we can get the post-program that can be recognized by a robot [26].

3. Experimental results and discussion

3.1. The influence of overlap modes on the coatings cracks and pores

Fig. 4 shows the cross-section morphology of specimens prepared by different overlap methods. It can be seen that the overlap mode has an obvious effect on the section defects of the specimen. The microstructure inhomogeneity of mode 1 is the worst, and the pores and cracks are also mainly concentrated in the overlapping zone, as shown in Fig. 4(a). Within overlap mode 2, it can be seen the pores and cracks are mainly concentrated in the overlap area, as shown in Fig. 4(b). The metallurgical bonding quality in the overlapping areas is worse than that of other parts, which may be caused by this problem. The possibility of defects in the overlapping area is high. With the continuous cladding, the internal stress increases, and cracks extend along with the defects such as slag inclusion and pores, which increases the crack quantity. The cross-section morphology of mode 3 (as shown in Fig. 4(c) has few pores and cracks in the clad layers. With a large remelting area along Z-axis, the surface of the solidified melted layer can be remelted, reduces the defects caused by the slag inclusion and incompletely melted particles in the overlapping zone, so as to improve the
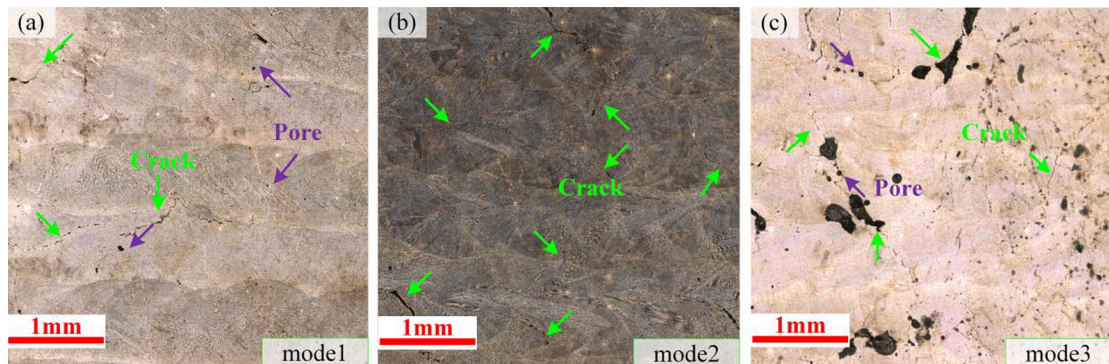

Fig. 4. Cross-section morphology of specimens. (a) mode 1; (b) mode 2; (c) mode 3.
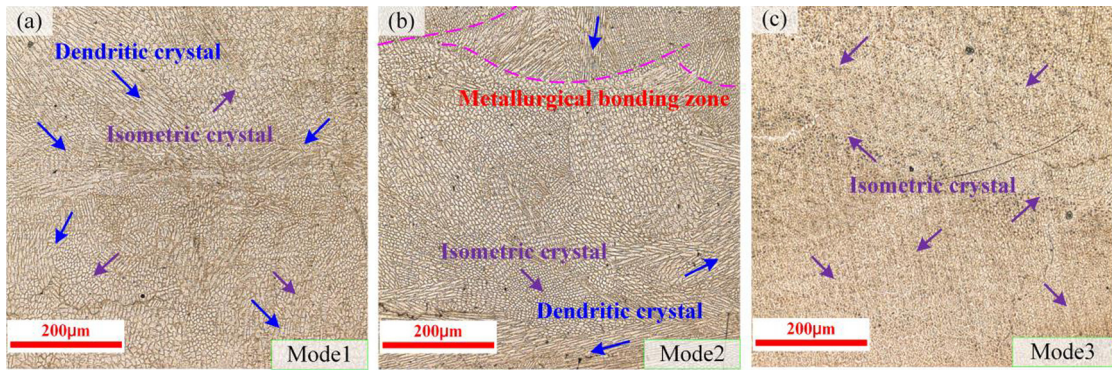
Fig. 5. Microstructure. (a) mode 1, (b) mode 2, (c) mode 3.

quality of interlayer metallurgy. The reasonable remelting area can make the powder bonded at the edge of the clad track remelt completely, thus generates the good metallurgical bonding at the overlapping zone.

Fig. 5 shows the effect of different overlap modes on the microstructure. Within the overlap Mode 1, columnar crystals mainly appear in the overlapping area between layers, and the direction of columnar crystals in the metallurgical bonding area is different. The microstructure of mode 2 is stratified obviously in the overlapping area. Although the microstructure in the metallurgical bonding area is still columnar crystals, the content, length, and area of columnar crystals are smaller than that of mode 1. The boundary of the molten pool is mainly fine isometric crystals. The metallurgical bonding zone of Mode 5 is dominated by isometric crystals and acicular dendrite crystals. The dendrite crystal region in all cross section of mode 5 is least, and compared with other methods, the grain size is smaller and the distribution is uniform.

3.2. Wear resistance analysis

Fig. 6 shows the test results of the YCF101 friction coefficient in 'vertical direction' (the specimens are perpendicular to the scanning direction) and 'horizontal direction' (the specimens are parallel to the scanning direction). Because of the fine micro-structure of mode3 in 'vertical direction', the friction coefficient fluctuates around 0.525 when wear is stable, and the friction coefficient of mode 2 and mode 1 in 'vertical direction' is 0.538 and 0.569 respectively. In 'horizontal direction', the overlap mode 1, mode 2 and mode 3, the homogeneity of the microstructure increases in turn, while the grain size decreases in turn. Therefore, during the wear process, the ability to resist the damage of external forces increases, and the friction coefficient of the specimen decreases relatively. The given order of friction coefficient: 0.576, 0.496 and 0.460. The friction coefficient of mode 1 which parallel to the scanning direction is higher than that of the vertical scanning direction, while that of mode 2 and 3 is the opposite. Within mode 1 (parallel to the scanning direction), the microstructure of the overlap zone is mainly columnar crystal and dendrite crystal, the grains are coarse, and the number of grains is small. While in the vertical direction, the dendrite and isometric crystals are mainly in the metallurgical bonding zone, and the number of grains is relatively increased. The homogeneity of the temperature distribution of mode 2 and 3 specimens is better in the horizontal clad layer. Different overlapping modes produce different remelting modes. The temperature field formed by mode 2 and 3 on the horizontal surface is more uniform than that formed vertically upward. Therefore, the homogeneity of microstructure and wear resistance of the clad layer is better. Different overlap modes did not change the composition and phase, but mainly changed the microstructure and grain size, and then the wear resistance of the clad layer is
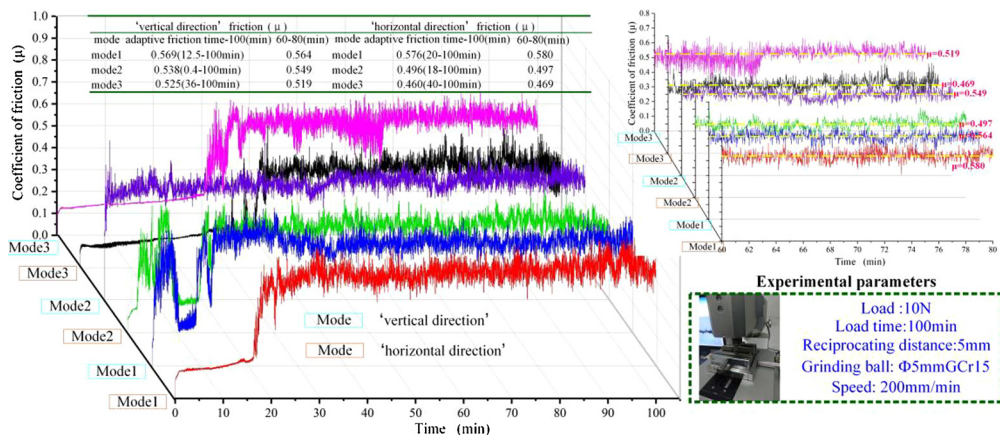

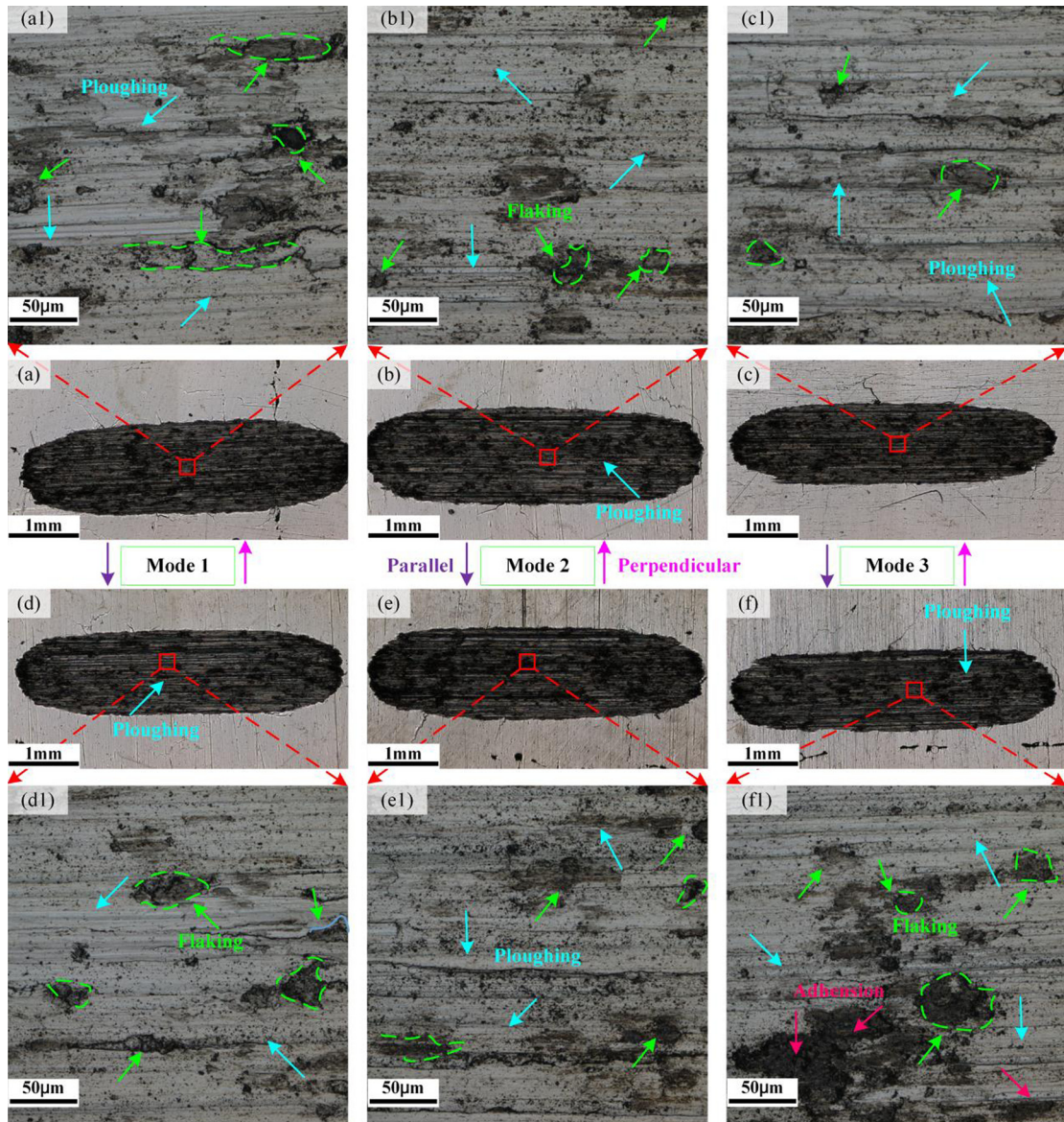**Fig. 6.** The specimens friction coefficient.

Fig. 7. Wear morphology. The specimens are perpendicular to the scanning direction: (a), (a1) mode1; (b), (b1) mode 2; (c), (c1) mode 3. The specimens are parallel to the scanning direction: (d), (d1) mode1; (e), (e1) mode 2; (f), (f1) mode 3.

changed.

Adhesive wear will occur when hard materials grind soft materials, usually two-body wear. The hardness of YCF101 powder is about 28HRC (provided by the merchant), while the hardness of the GCr15 ball is $60-66$HRC. Slight adhesion wear occurs on the surface of the specimen after wear, and a few flaking pits appear on the surface, but mainly plow-groove wear scars, as shown in Fig. 7. At the initial stage of wear, the microstructure is compact. With the continuous grinding, the polished surface is destroyed, and the temperature and stress continue to increase, then fatigue wear, sub-surface fracture, and flaking pits will occur. Macroscopically, the wear scar width of Mode 3 is smaller than that of the other two modes. The flaking pit also decreases with the increase of the complexity of overlap mode between layers. Temperature field distribution can be controlled by changing overlap mode, and then controls the homogeneity of the microstructure. The composition and phase of the clad layer are not changed. The grain size and homogeneity of microstructure play a decisive role in the wear properties of the clad layers obtained by experiments.

Fig. 8 illustrates the effect of overlap mode on the cross section morphology of wear scar (the specimens are parallel to the scanning direction). The depth and width of wear scar in mode 3 is small, mainly due to the fine microstructure, which increases the force to destroy the grain boundaries. The depth of the wear scar is about 20 μm.

The cross section morphology of wear scar along z-axis shows that the depth of wear scars is greater than that in 'horizontal direction'. The depth of wear scars is about 35 μm, and the value of mode 3, 2 and 1 increases in turn, as shown in Fig. 9. The width in
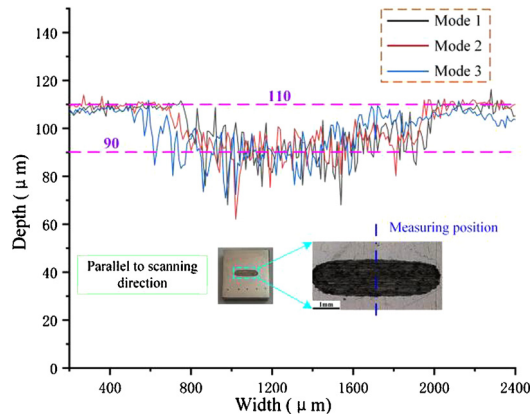
Fig. 8. Cross-section morphology of wear marks along scanning direction.
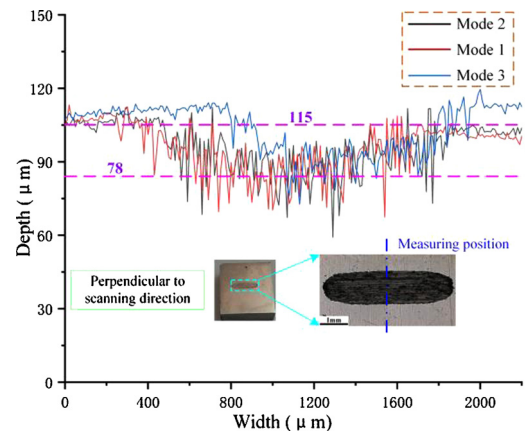

Fig. 9. Cross-section morphology of wear marks along z-axis.

the 'vertical direction' (the specimens are perpendicular to the scanning direction) is smaller than that in the 'horizontal direction'. The main reason is that the degree of non-uniformity of the microstructure in the 'vertical direction' is greater than that in the 'horizontal direction'. The grain density in the molten pool is higher and the temperature is the highest. When the longitudinal overlap occurs, the microstructure in the overlapping zone is larger than that in the molten pool, and the interlaced dendrites crystal increase the non-uniformity. The adhesion is not obvious, and the wear scars are deep and narrow. In the 'horizontal direction', the layer can be remelted in a different direction when several layers near this layer are cladded using different laser cladding direction. With the continuous growth of the grains, the microstructure of the cladding layer in the cladding plane becomes uniformity and the size of the grains becomes small. It is more difficult to wear the worn surface and the wear scar is shallow. However, during the wear process, the adhesion is relatively serious compared with the 'vertical direction', and the steel ball has slight wear, resulting in a wide friction surface, generating a wide friction surface.

3.3. Compressive strength measurement and analysis

Compressive strength is one of the important macroscopic characteristics of the laser cladding layer, which can be evaluated by the stress-strain curve. In order to intuitively and truly reflect the compressive performance of the parts under each overlap mode, the loading rate of 2 mm/min was used in compression experiments under static load displacement control at room temperature of 16 degrees Celsius. The stress-strain curves of the specimens are shown in Fig. 10. Most of the specimens have no maximum load, i.e. no maximum compressive strength. The compressive properties of specimens prepared along the z-axis direction are better than those along the scanning direction. The compressive strength of specimens under different overlap modes is as follows: mode 1 (along z-axis direction), mode 3 (along z-axis direction), mode 1 (along scanning direction), mode 3 (along scanning direction) and mode 2 (along scanning direction). The main reason is that the mode 1 cladding direction is the same, and the high consistency of grain growth direction generates better compressive performance under external pressure. When mode 3 is used, the uniformity of the structure and grain number is improved, so the compressive property is high. The wave in the curve is mainly the compaction stage of the sample in the compression process. The compressive resistance of the clad track as the stress surface is higher than that of the cross section of the clad track as the stress surface. The quality of the overlap zone is weak. When the cross-section of the clad track acts as
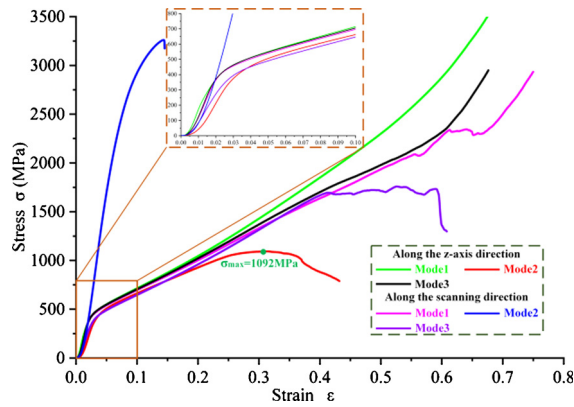
Fig. 10. Stress-strain curve of specimen.

the stress surface, the overlap mode of different angles increases the area of the sharp angle between the overlap zone and the stress direction. Thus, it is not conducive to improving the compressive strength of the clad layers.

After yielding, the compression curve increases with the pressure, and the specimen is finally pressed into a thin sheet without fracture, as shown in Fig. 11. YCF101 alloy is a plastic material with no strength limit under compression. According to Fig. 11, it can be seen that with the increase of overlap mode complexity, the damage degree of the sample decreases in turn after crushing. The higher homogeneity of the structure and the finer and more compact grain play an important role in the cladding layer compressive strength.

4. Conclusions

The study investigated the effect of overlap mode on the YCF101 alloy clad layer quality (crack and pore), wear resistance, microhardness and strength. From comparison and analysis, the following conclusions according to the above experiments are shown:

(1) The overlap mode can effectively control the cracks and pores in the clad layers. With the increase of remelting area, the uniformity of remelting temperature distribution increases, the cranks and pores decreases and the microstructure fineness increases.

(2) Compared with the z-axis direction, the friction coefficient along the scanning direction is low, and the wear scars are shallow and narrow. The grinding depth decreased by 46 % from about 37 μm to about 20 μm. With the increase of overlap mode complexity (from mode 1 to mode 3), wear resistance decreases gradually, and wear scar width decreases. Along the scanning direction, the friction coefficient decreases from 0.576 to 0.46, while along the z-axis, the value decreases from 0.569 to 0.525.

(3) YCF101 is a plastic material, and the uniformity of grain can improve the compressive properties of the clad layer. The compressive resistance of the clad track as the stress surface is higher than that of the cross section of the clad track as the stress surface. When the cross section of the clad track acts as the stress surface, the worse the uniformity of the clad track along the stress direction is, the worse the compressive capacity is.

Declaration of Competing Interest

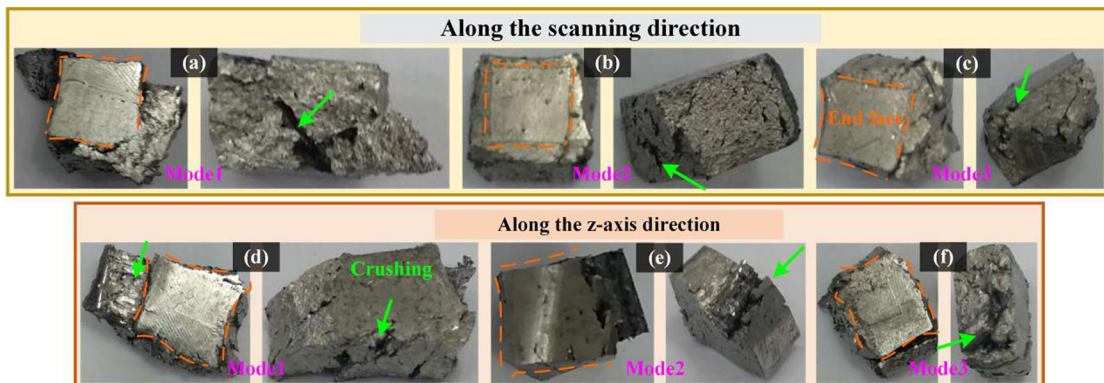The authors declare that there are no conflicts of interest.

Fig. 11. Crush morphology.

Acknowledgment

References

[1] J. Zeisig, N. Schädlich, L. Giebeler, J. Sander, J. Eckert, U. Kühn, J. Hufenbach, Microstructure and abrasive wear behavior of a novel FeCrMoVC laser cladding alloy for high-performance tool steels, Wear 382–383 (2017) 107–112, https://doi.org/10.1016/j.wear.2017.04.021.
[2] Q. Lai, R. Abrahams, W. Yan, C. Qiu, P. Mutton, A. Paradowska, X. Fang, M. Soodi, X. Wu, Effects of preheating and carbon dilution on material characteristics of laser- cladded hypereutectoid rail steels, Mater. Sci. Eng. A 712 (2018) 548–563.
[3] H. Zhang, K. Xin, J. Liang, J. Liu, Microstructure and mechanical properties investigations of copper-steel composite fabricated by explosive welding, Mater. Sci. Eng. A 731 (2018) 278–287.
[4] Y. Lyu, Y. Sun, F. Jing, On the microstructure and wear resistance of Fe-based composite coatings processed by plasma cladding with B4C injection, Ceram. Int. 41 (2015) 10934–10939, https://doi.org/10.1016/j.ceramint.2015.05.036.
[5] Y. Guo, Z. Li, C. Yao, K. Zhang, F. Lu, K. Feng, J. Huang, M. Wang, Y. Wu, Microstructure evolution of Fe-based nanostructured bainite coating by laser cladding, Mater. Des. 63 (2014) 100–108, https://doi.org/10.1016/j.matdes.2014.05.041.
[6] L. Fan, H. yan Chen, Y. hua Dong, L. hua Dong, Y. sheng Yin, Wear and corrosion resistance of laser-cladded Fe-based composite coatings on AISI 4130 steel, Int. J. Miner. Metall. Mater. 25 (2018) 716–728, https://doi.org/10.1007/s12613-018-1619-2.
[7] S.R. Lewis, R. Lewis, P.S. Goodwin, S. Fretwell-Smith, D.I. Fletcher, K. Murray, J. Jaiswal, Full-scale testing of laser clad railway track; case study–testing for wear, bend fatigue and insulated block joint lipping integrity, Wear 376–377 (2017) 1930–1937, https://doi.org/10.1016/j.wear.2017.02.023.
[8] S.R. Lewis, R. Lewis, P.S. Goodwin, D.I. Fletcher, K. Murray, PPT_Improving Rail Wear and RCF Performance Using Laser Cladding 4 (2015).
[9] R. Khatib, Z. Davani, R. Miresmaeili, M. Soltanmohammadi, Effect of thermomechanical parameters on mechanical properties of base metal and heat affected zone of X65 pipeline steel weld in the presence of hydrogen, Mater. Sci. Eng. A 718 (2018) 135–146.
[10] Z. Weng, A. Wang, Y. Wang, D. Xiong, H. Tang, Diode laser cladding of Fe-based alloy on ductile cast iron and related interfacial behavior, Surf. Coat. Technol. 286 (2016) 64–71, https://doi.org/10.1016/j.surfcoat.2015.12.031.
[11] X. Jiao, J. Wang, C. Wang, Z. Gong, X. Pang, S.M. Xiong, Effect of laser scanning speed on microstructure and wear properties of T15M cladding coating fabricated by laser cladding technology, Opt. Lasers Eng. 110 (2018) 163–171, https://doi.org/10.1016/j.optlaseng.2018.05.024.
[12] W. Gao, S. Zhao, F. Liu, Y. Wang, C. Zhou, X. Lin, Effect of defocus manner on laser cladding of Fe-based alloy powder, Surf. Coat. Technol. 248 (2014) 54–62, https://doi.org/10.1016/j.surfcoat.2014.03.019.
[13] T. Roy, Q. Lai, R. Abrahams, P. Mutton, A. Paradowska, M. Soodi, W. Yan, Effect of deposition material and heat treatment on wear and rolling contact fatigue of laser cladded rails, Wear 412–413 (2018) 69–81, https://doi.org/10.1016/j.wear.2018.07.001.
[14] Z.K. Fu, H.H. Ding, W.J. Wang, Q.Y. Liu, J. Guo, M.H. Zhu, Investigation on microstructure and wear characteristic of laser cladding Fe-based alloy on wheel/rail materials, Wear 330–331 (2015) 592–599, https://doi.org/10.1016/j.wear.2015.02.053.
[15] X. Lei, C. Huajun, L. Hailong, Z. Yubo, Study on laser cladding remanufacturing process with FeCrNiCu alloy powder for thin-wall impeller blade, Int. J. Adv. Manuf. Technol. 90 (2017) 1383–1392, https://doi.org/10.1007/s00170-016-9445-z.
[16] C.M. Lin, Parameter optimization of laser cladding process and resulting microstructure for the repair of tenon on steam turbine blade, Vacuum 115 (2015) 117–123, https://doi.org/10.1016/j.vacuum.2015.02.021.
[17] H. Zhang, Y. Zou, Z. Zou, D. Wu, Microstructure and properties of Fe-based composite coating by laser cladding Fe-Ti-V-Cr-C-CeO2 powder, Opt. Laser Technol. 65 (2015) 119–125, https://doi.org/10.1016/j.optlastec.2014.06.016.
[18] W. Gao, S. Zhao, Y. Wang, Z. Zhang, C. Zhou, X. Lin, Refinement of Fe-based alloy doped Ti cladding layer, Surf. Coat. Technol. 270 (2015) 16–23, https://doi.org/10.1016/j.surfcoat.2015.03.024.
[19] M. Zhang, K.L. Qu, S.X. Luo, S. Xia, Effect of Cr on the microstructure and properties of TiC-TiB2particles reinforced Fe-based composite coatings, Surf. Coat. Technol. 316 (2017) 131–137, https://doi.org/10.1016/j.surfcoat.2017.03.026.
[20] Q. Li, Y. Lei, H. Fu, Growth characteristics and reinforcing behavior of in-situ NbCp in laser cladded Fe-based composite coating, J. Mater. Sci. Technol. 31 (2015) 766–772, https://doi.org/10.1016/j.jmst.2014.06.012.
[21] H. Zhang, Y. Zou, Z. Zou, C. Shi, Effects of chromium addition on microstructure and properties of TiC-VC reinforced Fe-based laser cladding coatings, J. Alloys Compd. 614 (2014) 107–112, https://doi.org/10.1016/j.jallcom.2014.06.073.
[22] Q. Li, Y. Lei, H. Fu, Growth mechanism, distribution characteristics and reinforcing behavior of (Ti, Nb)C particle in laser cladded Fe-based composite coating, Appl. Surf. Sci. 316 (2014) 610–616, https://doi.org/10.1016/j.apsusc.2014.08.052.
[23] S. Chen, H. Hu, M. Zhao, L. Rong, Effect of post-weld aging treatment on the precipitation and mechanical behavior of Fe-Ni based alloy weldment, Mater. Sci. Eng. A 718 (2018) 363–370.
[24] T. Yu, Y. Zhao, J. Sun, Y. Chen, W. Qu, Process parameters optimization and mechanical properties of forming parts by direct laser fabrication of YCF101 alloy, J. Mater. Process. Technol. 262 (2018) 75–84, https://doi.org/10.1016/j.jmatprotec.2018.06.023.
[25] Y. Zhao, T. Yu, J. Sun, W. Xi, X. Bi, Effect of laser cladding on forming qualities of YCF101 alloy powder in the different lap joint modes, Int. J. Adv. Manuf. Technol. 96 (2018) 1991–2001, https://doi.org/10.1007/s00170-018-1732-4.
[26] Y. Zhao, T. Yu, B. Li, Z. Wang, H. Chen, Calculation and verification of Start/Stop optimum overlapping rate on metal DLF technology, Int. J. Adv. Manuf. Technol. (2018) 437–452, https://doi.org/10.1007/s00170-018-2445-4.
[27] T. Yu, J. Sun, W. Qu, Y. Zhao, L. Yang, Influences of z-axis increment and analyses of defects of AISI 316L stainless steel hollow thin-walled cylinder, Int. J. Adv. Manuf. Technol. 97 (2018) 2203–2220, https://doi.org/10.1007/s00170-018-2083-x.